ISSN 0021-3640, JETP Letters, 2024, Vol. 119, No. 9, pp. 665–671. © Pleiades Publishing, Ltd., 2024.
Russian Text © The Author(s), 2024, published in Pis'ma v Zhurnal Eksperimental'noi i Teoreticheskoi Fiziki, 2024, Vol. 119, No. 9, pp. 651–657.

OPTICS
AND LASER PHYSICS

Time-Resolved Detection of Terahertz Response in Photodynamically Induced Plasmonic Metasurfaces

I. A. Novikov[a] (ORCID: 0000-0002-7652-7816), M. A. Kiryanov[a] (ORCID: 0000-0002-4534-3491), V. I. Stadnichuk[a], T. V. Dolgova[a] (ORCID: 0000-0001-8981-0808), and A. A. Fedyanin[a,*] (ORCID: 0000-0003-4708-6895)

[a] *Faculty of Physics, Moscow State University, Moscow, 119991 Russia*

**e-mail: fedyanin@nanolab.phys.msu.ru*

Received March 27, 2024; revised April 5, 2024; accepted April 7, 2024

A modification of terahertz time-domain spectroscopy is proposed. It includes the direct measurement of the temporal profile of the transmitted terahertz pulse, the extraction of the pulse corresponding to multiple reflections from the object surfaces, and its analysis without the Fourier transform algorithm. The method is tested on one-dimensional gratings that are photodynamically induced on the gallium arsenide surface and support the excitation of collective plasmonic modes in the terahertz range. The suggested approach allows us to overcome the limitations typical of the conventional terahertz time-domain spectroscopy and expands the capabilities of the existing terahertz photonic instrumentation.

DOI: 10.1134/S0021364024601052

One of the main experimental methods in terahertz (THz) photonics is THz time-domain spectroscopy (THz-TDS) [1]. The technique is applicable to a wide range of scientific tasks [2] including the study of molecular vibrations [3], phase transitions [4, 5] and elementary excitation [6–8] in solids, and material characterization [9, 10], i.e., the determination of the material constants (refractive index, absorption coefficient, conductivity) in the THz range from the object reflectance or transmittance. Terahertz time-domain spectroscopy allows one to characterize a great number of various materials including semiconductors [11], superconductors [12], ferroelectrics [13], topological insulators [14], polymers [15], liquids [10], solutions [16], and biological tissues [17]. Such a great number of studied objects and scientific problems stimulated the development of THz-TDS. As a result, a method for studying the materials with high absorption [18], novel approaches to improve the sensitivity of detection [19, 20], and the nonlinear THz spectroscopy technique [21] were developed. Nevertheless, the THz-TDS technique has a number of features that affect the accuracy of the results obtained and limit its application in some cases.

Since THz-TDS utilizes the Fourier transform algorithm, the output spectrum of the signal depends on the measurement parameters (duration, step size, window function, etc.) [22]. Moreover, multiple reflections from the sample facets cause the appearance of additional features in temporal response or oscillations in the spectrum [23]. The oscillations become significant in the case of even the only additional reflection. Multiple reflections are parasitic factor for THz-TDS that needs to be removed [24] or taken into account during the post-processing [25, 26]. Finding geometries that allows one to avoid multiple reflections can be challenging [27].

A search for novel methods to control THz radiation is one of the relevant area of THz photonics. The control of the wavelength, frequency, phase, a change in polarization and propagation direction are the examples of the problems that need to be solved. The mentioned transformations can be realized with the help of metamaterials and metasurfaces – artificial three- and two- dimensional structures constituted by ordered subwavelength elements [28]. A specific organization leads to the appearance of properties inherent neither to the material itself, nor to a constituting block [29, 30]. Moreover, metamaterials and metasurfaces can support the excitation of resonant electromagnetic modes of various types [31–35], that allows one to trap the incident radiation and localize it at the interface. As a result, the performance of the metastructure drastically increases. Such resonant electromagnetic excitations include, in particular, various plasmonic modes [36–39]. The concept of plasmonic metamaterials and metasurfaces has become widespread in optics [40] and is now developing in terahertz photonics [41, 42].

Terahertz metamaterials and metasurfaces are usually passive. Their properties remain fixed after manufacturing and can be tuned only within small limits by

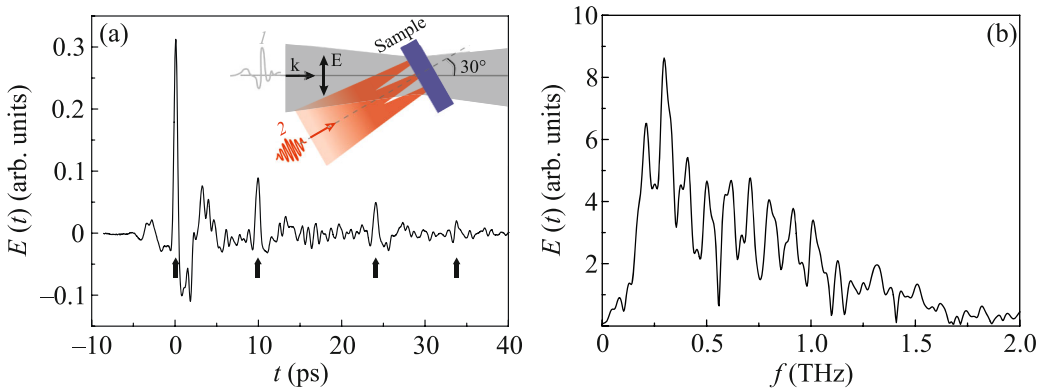

Fig. 1. (Color online) (a) Temporal profile and (b) spectrum of the THz pulse transmitted through the GaAs plate in the absence of optical pumping. Here and in other figures, the time is measured from the maximum of the main THz pulse. The inset shows the ray paths to the sample: (*1*) THz and (*2*) pump pulses and (**k**, **E**) THz pulse propagation and polarization directions, respectively.

external stimuli, which significantly reduce the metastructure capabilities. In this regard, research aimed at development of active THz metamaterials are carried out [43]. The authors of [27] proposed a method allowing the generation of a submillimeter-scale arbitrary-shaped spatial charge distribution on a flat semiconductor surface by femtosecond laser radiation due to the photoelectric effect. The charge distribution completely follows the modulated spatial profile of optical illumination obtained using masks [44], a spatial light modulator (SLM) [27, 45] or projectors [46, 47]. The method, named photodynamic or photoinduced generation, allowed the implementation of various active photonic elements suitable for THz range including tunable filters [48], beam steering devices [46], polarizers [47], waveguides [49], modulators integrated into THz imaging systems [45, 50, 51], diffraction gratings [52] and more complex THz metasurfaces [53]. The excitation of plasmonic modes in photodynamically induced THz structures was shown for randomly distributed particles (submillimeter antennas) [54], but not for metasurfaces.

In this paper, the modification of terahertz time-domain spectroscopy is proposed. The idea lies in the direct measurement of the temporal signal corresponding to the field of the THz pulse transmitted through the sample. Two parts are distinguished from the signal. The first one corresponds to the pulse transmitted directly through the sample, the second one is the pulse reflected twice from its surfaces. Both pulses are analyzed without the use of Fourier transform algorithm. The proposed method is applied to the study of one-dimensional gratings photoinduced on a flat gallium arsenide surface by the structured laser illumination and supporting the excitation of surface plasmon in the THz range.

A 400-μm-thick high-resistivity gallium arsenide plate was used as a substrate for photoinduced generation of one-dimensional gratings by focusing a spatially modulated 800-nm femtosecond pulse. The hundreds-of-microns grating pitch matched the available spectral range of THz radiation. A computer-generated hologram (CGH) was displayed onto phase-only reflective SLM Holoeye Pluto-2.1 NIR and was then optically reconstructed on the GaAs surface. The computer-generated holograms were obtained using an inverse 2D Fourier transform algorithm on the target projection image. Two types of images were used: solid (homogeneous) rectangle covering all active area of SLM and one-dimensional gratings with different pitch values and strip orientations. We used the first group of images for calibration and the second one for the main experiment.

A regeneratively amplified Ti: sapphire laser with a 800-nm central wavelength, 50-fs pulse duration, 1 kHz repetition rate and 3 mJ pulse energy was used as a source of radiation. The initial pulse was split on two consecutive beam splitters into three beams: generating, probe and pump. The intensity ratio of the beams was 63:3:33, respectively. The first (generating) pulse was used to generate THz radiation (0.25–2 THz) by optical rectification in a 0.5-mm-thick ZnTe crystal. Generated THz radiation was then focused onto the sample surface by two parabolic mirrors. The electric field of the transmitted THz pulse was measured with probe beam by the electro-optical sampling method in conventional THz-TDS scheme [2]. Pump beam was used to reconstruct the CGH image on the sample surface. The illuminated areas supported the generation of free carriers. The GaAs sample was positioned normally to the incident pump beam. The THz pulse was incident on the sample surface at an angle of 30° and was polarized in the plane of incidence (see the inset of Fig. 1a).

Figure 1a shows the electric field temporal profile of the THz pulse transmitted through the sample in the absence of optical illumination. The complex shape signal with a great number of oscillations and

four pronounced peaks at the delays of 0, 9.8, 24, and 33.7 ps is observed. The shape in the vicinity of each peak coincides up to a constant factor. It allows us to assume that at least four separate THz pulses are observed and three of them copy the first one. The copies appear as a result of multiple reflections from the surfaces of the sample and ZnTe used for THz generation. The both are plates with two parallel reflecting surfaces. Thus, a peak at the 9.8-ps delay corresponds to the THz pulse directly transmitted though the ZnTe crystal and reflected consequently from the rear and the front surfaces of the sample. Peak at the 24-ps delay corresponds to the THz pulse reflected twice from the facets of nonlinear crystal and then directly transmitted though the studied sample. Finally, peak at 33.7-ps delay corresponds to the pulse reflected twice from rear and front facets of both ZnTe crystal and the sample. THz pulses that reflect more than twice have significantly less amplitudes and are indistinguishable from random noise and oscillations.

Figure 1b shows the spectrum of the THz pulse transmitted through the unpumped sample. Complex-shaped oscillations are observed. Shifted copies of the main THz pulse in the measured time-domain signal lead to the appearance of the oscillations. According to time shifting property of Fourier transform, the Fourier spectrum of the shifted signal is the same as that of the original signal up to an oscillating term $e^{-i\omega\Delta\tau}$, where $\Delta\tau$ is a time delay between both signals. The use of spectral data presented in Fig. 1b to determine the real part of refractive index n and absorption coefficient α of the material in THz range is difficult and requires extensive processing.

Both indices n and α can be found directly from the analysis of time delay and amplitude of the THz pulse reflected from both surfaces of the sample. Hereinafter this pulse is called a satellite. A peak in the time-domain signal, that corresponds to the satellite, is delayed relative to the main pulse by $\Delta t = 9.8$ ps. Since the sample thickness is 400 μm, the angle of incidence of THz radiation to sample surface is 30° the real part of non-radiated sample refractive index n can be found to be 3.64. The determined value is close to that presented in literature [11]. The absorption coefficient α can be found from comparison of the main and satellite pulses amplitudes. The decrease in the latter amplitude is governed by either reflection from the media with different refractive indices or by the internal absorption. Thus, the main and satellite amplitudes ratio can be found using the following equation:

$$\frac{E_m}{E_{\text{sat}}} = \frac{1}{r^2 e^{-2\alpha d}}, \quad (1)$$

where r is the amplitude reflection coefficient at the air–sample interface, α corresponds to an absorption coefficient of the sample, d is its thickness. Knowing the E_m/E_{sat} value from Fig. 1a, sample thickness d and its refractive index n found earlier, one can calculate α. The E_m/E_{sat} value in our case is $0.31/0.085 \approx 3.64$. The value of r coefficient calculated from Fresnel equations for the given n is 0.525. Then $1/r^2$ is around 3.63 that is close to E_m/E_{sat} value. It means that $e^{-2\alpha d} \to 1$. Thus, the absorption coefficient of unpumped gallium arsenide is quite low which is also consistent with the results of the previous work [11]. Note that both material constants n and α were determined without the use of Fourier transform algorithm and the results of the reference measurement with no sample.

The proposed approach is used to study the response of one-dimensional gratings photodynamically induced on the gallium arsenide surface and supporting the plasmon excitation in THz range. The experiment is conducted as follows. Images of one-dimensional gratings with various pitch values are reconstructed on the surface of gallium arsenide plate. The orientation of the grating strips and the pump pulse power are chosen to fulfill the condition of surface plasmon excitation. Thus, an orthogonal to the plane of incidence and THz pulse polarization orientation is used. The pump pulse fluence is taken to be 30 μJ/cm^2. Calibration measurements with homogeneous illumination reveal that a laser pulse with the given fluence induces a free charge carrier density of 5×10^{17} cm^{-3}. The estimation is based on a method proposed in [55]. The photoinduced carrier density N_{pc} in one-dimensional rectangular grating with 50% fill factor will be twice as high, 10^{18} cm^{-3}. The analytical calculation based on the Drude model shows that the value of dielectric permittivity (real part) ϵ'_{eff} in an area of plasmon localization for such a value of carrier density is equal to -8.1. The permittivity value is enough to fulfill the condition of plasmon excitation at the irradiated sample–air interface ($\epsilon'_{\text{eff}} < -\epsilon_d$, where $\epsilon_d = 1$). The period of photoinduced rectangular gratings is varied from 280 to 2100 μm. The frequency of diffraction anomalies for gratings periods within this range and for the used angle of incidence (30°) will fall within the spectral range of generated THz radiation (0.25–2 THz).

As in the case of non-radiated gallium arsenide, the time-domain temporal waveform of the transmitted THz pulse is measured, from which the part corresponding to the satellite electric field is extracted. Figure 2a shows temporal profiles of satellite electric fields $E(t)$ for photoinduced gratings with various periods d. Multiple interference causes the complex line shape of the detected signals. Waves reflecting from the gallium arsenide–air interface as well as these interacting with the pump-induced gradient medium inside the semiconductor take part in the interference. As a result, the peak of satellite field in the time-domain signal in the vicinity of 10-ps delay is trans-

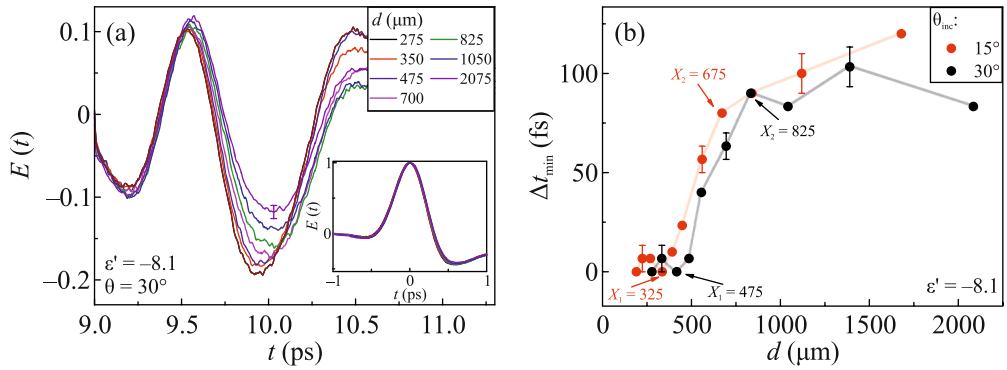

Fig. 2. (Color online) (a) Temporal profile of the satellite electric field $E(t)$ in photoinduced gratings with various periods d. All curves are normalized to the maximum field of the main pulse. The inset shows the normalized field of the main pulse. (b) Satellite field minimum shift Δt_{min} versus the spatial period d of photoinduced gratings for two angles of incidence of the THz pulse. The pump fluence was 30 μJ/cm^2. The grating strips are perpendicular to the polarization of the THz pulse.

formed into a dip. It is seen (Fig. 2a) that an increase in the period of photoinduced gratings leads to a decrease in the dip amplitude and its shift towards longer time delays. Dependence of the satellite field minimum shift Δt_{min} on the period of photoinduced gratings d for the given angle of incidence of the THz pulse (30°) is shown by black curve in Fig. 2b. Within all the range of period change (275–2075 μm) the minimum is shifted by about 100 fs. The shift is non-monotonic: up to 475-μm period the satellite field minimum position t_{min} is constant but at higher periods it starts to grow rapidly. The rapid growth lasts till the period of 825 μm. Further increase in period d has almost no effect on t_{min}.

The period of grating photoinduced on sample surface primarily affects the frequencies of diffraction (for instance, Rayleigh anomaly) and plasmonic (phase synchronism condition) anomalies. The amplitudes of interfering waves that form the satellite temporal profile depend slightly on the grating period but are rather affected by its fill factor and the pump power. Both parameters are fixed in the experiment. It allows us to propose a diffraction nature of the observed effect. To test it out, we repeat the experiment and measure the dependence of Δt_{min} on the period d of photoinduced gratings for different angles of incidence θ_{inc} provided that all other grating parameters (ϵ', fill factor, strip orientation) are fixed. The measured dependence is shown in Fig. 2b for angles of incidence of 15° and 30°. It is seen that the change in the angle of incidence led to a shift of the dependence. The grating period, from which the dip modification in time-domain waveform (Fig. 2a) and the appearance of an inflection point in the dependence of Δt_{min} on d (Fig. 2b) were observed decreased from 475 to 325 μm.

The found results are interpreted as follows. The satellite profile changes when its spectrum overlaps with d-dependent Rayleigh anomaly. Inflection points in the dependence of Δt_{min} on d (see Fig. 2b) correspond to grating periods at which the frequency of Rayleigh anomaly falls on satellite spectrum edges. Thus, the first inflection point is observed at the periods of 325 and 475 μm for angles of THz incidence of 15° and 30°, respectively. The frequency f_R of the first order Rayleigh diffraction anomaly can be calculated by the formula

$$f_R = \frac{c}{d(1 - \sin\theta_{inc})}. \quad (2)$$

Since the satellite spectrum is defined by the source of THz radiation and thus does not change between experiments, the calculated f_R values for both periods (325 and 475 μm) should be equal. The f_R value calculated using Eq. (2) for d = 325 μm and $\theta_{inc} = 15°$ is 1.25 THz. The f_R value for $d = 475$ μm and $\theta_{inc} = 30°$ is 1.26 THz. The concurrence of both calculated f_R values confirms the diffraction nature of the observed satellite field profile modification. The second inflection point in the dependence shown in Fig. 2b which corresponds to the lower frequency edge of the satellite spectrum is observed at $d = 675$ and 825 μm for angles of incidence 15° and 30°, respectively. It is seen (mostly pronounced for 15° case) that for periods above this edge where there is no overlap between satellite spectrum and Rayleigh anomaly, the dip keeps shifting. The influence of surface plasmons whose spectra are significantly wider than those of Rayleigh anomalies can cause such an effect.

To distinguish diffraction and plasmonic mechanisms one has to use the geometries that do not support the excitation of surface plasmons. They will not be excited in the gratings with the strip orientation collinear to the polarization of the incident THz pulse and the plane of incidence. Figure 3 shows the satellite minimum shift Δt_{min} with the period d for photoin-

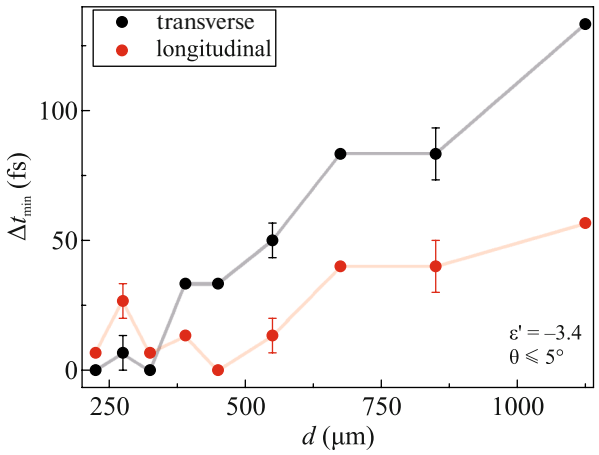

Fig. 3. (Color online) Satellite field minimum shift Δt_{min} versus the period d of photoinduced gratings for the transverse (plasmonic) and longitudinal (non-plasmonic) strip orientations. The THz pulse is incident almost normally to the sample surface.

duced gratings with the transverse (plasmonic) and longitudinal (non-plasmonic) strip orientations. The same fluence (23 μJ/cm^2) is used in both experiments, and the THz pulse is incident almost normally to the sample surface ($\theta_{inc} \leq 5°$). The Δt_{min} range for the grating with the transverse strip orientation is around 133 fs. It is almost 2.7 times larger than that for the grating with longitudinal strips (50 fs). The satellite profile is modified when its spectrum overlaps with period-dependent diffraction and plasmonic anomalies. A grating with the transverse strip orientation supports both types of anomalies while a grating with longitudinal strips only the diffraction ones. Since the spectrum of plasmonic resonance is significantly wider than that of the Rayleigh anomaly, overlapping will be observed within the larger range of periods and cause higher Δt_{min} that is exactly what is seen in Fig. 3. Diffraction effects allow one to shift the delay corresponding to the satellite dip by 50 fs (red line in Fig. 3) within the range of studied periods (225–1125 μm). Additional 80-fs shift is caused by the excitation of surface plasmons (a difference between black and red lines in Fig. 3).

Note that the change in photoinduced gratings period has almost no effect on the main pulse (see the inset of Fig. 2a) but affects drastically the satellite. It can be attributed to a greater plasmonic contribution in the second case. The plasmon excitation efficiency and their spectrum are both affected by the grating profile [56]. In our case the profiles of photoinduced gratings differ relative to the propagation direction of the THz pulse (air → GaAs or GaAs → air). Thus, the spectra of main (transmitted directly) and satellite (reflected twice) pulses are different. Finding two unknown spectra from the same time-domain signal using the Fourier transform will lead to an ambiguous results. It means that the use of conventional post-processing methods based on the inclusion of the secondary multiple-reflection peaks in the time-domain signal [25, 26] under the conditions of propagation asymmetry may lead to incorrect results.

In conclusion, a modification of THz time-domain spectroscopy has been proposed. It includes the direct measurement of the temporal waveform of the transmitted THz pulse, the extraction of the part corresponding to the pulse reflected twice from both sides (front and rear) of the object and the subsequent analysis without the Fourier-transform algorithm. Submillimeter one-dimensional gratings photoinduced on a flat gallium arsenide surface by the structured laser illumination have been studied using the proposed method. The possibility to excite the collective plasmonic modes in such objects has been demonstrated. The developed approach allows one to overcome the disadvantages of the THz-TDS technique, complementing and expanding its opportunities. Moreover, the conventional methods based on the use of the Fourier transform algorithm are not applicable to photodynamically induced THz metasurfaces due to the asymmetry of their surface shape relative to the direction of beam propagation. The spectra of the pulses directly transmitted through the sample and several times reflected from its surfaces are different. Therefore, the use of conventional post-processing methods based either on the elimination of secondary peaks in the time-domain signal or on their inclusion similarly to the multiple reflections in Fabry–Perot interferometers may lead to incorrect results.

ACKNOWLEDGMENTS

The experiments were carried out with the equipment provided under the development program of the Moscow State University.

FUNDING

This work was supported by Russian Science Foundation, project no. 20-12-00371. M.A. Kiryanov acknowledges the support of the Foundation for the Advancement of Theoretical Physics and Mathematics BASIS.

CONFLICT OF INTEREST

The authors of this work declare that they have no conflicts of interest.

REFERENCES

1. M. C. Nuss and J. Orenstein, in *Millimeter and Submillimeter Wave Spectroscopy of Solids*, Ed. by G. Grüner (Springer, Berlin, 1998).
2. P. Y. Han and X.-C. Zhang, Meas. Sci. Technol. **12**, 1747 (2001).

3. M. Walther, P. Plochocka, B. Fischer, H. Helm, and P. Uhd Jepsen, Biopolymers **67**, 310 (2002).
4. P. U. Jepsen, B. M. Fischer, A. Thoman, H. Helm, J. Y. Suh, R. Lopez, and R. F. Haglund, Phys. Rev. B **74**, 205103 (2006).
5. K. Makino, K. Kato, Y. Saito, P. Fons, A. V. Kolobov, J. Tominaga, T. Nakano, and M. Nakajima, J. Mater. Chem. C **7**, 8209 (2019).
6. T. Suzuki and R. Shimano, Phys. Rev. Lett. **103**, 057401 (2009).
7. G. Li, Z. Jin, X. Xue, X. Lin, G. Ma, S. Hu, and N. Dai, Appl. Phys. Lett. **100**, 191115 (2012).
8. K. Grishunin, T. Huisman, G. Li, E. Mishina, T. Rasing, A. V. Kimel, K. Zhang, Z. Jin, S. Cao, W. Ren, G.-H. Ma, and R. V. Mikhaylovskiy, ACS Photon. **5**, 1375 (2018).
9. M. Hangyo, M. Tani, and T. Nagashima, Int. J. Infrared Millim. Waves **26**, 1661 (2005).
10. J. T. Kindt and C. A. Schmuttenmaer, J. Phys. Chem. **100**, 10373 (1996).
11. D. Grischkowsky, S. Keiding, M. van Exter, and C. Fattinger, J. Opt. Soc. Am. **7**, 2006 (1990).
12. R. Matsunaga, Y. I. Hamada, K. Makise, Y. Uzawa, H. Terai, Z. Wang, and R. Shimano, Phys. Rev. Lett. **111**, 057002 (2013).
13. V. Bilyk, E. Mishina, N. Sherstyuk, A. Bush, A. Ovchinnikov, and M. Agranat, Phys. Status Solidi RRL **15**, 2000460 (2021).
14. K. A. Kuznetsov, P. I. Kuznetsov, A. D. Frolov, A. M. Konovalov, P. M. Kovaleva, and G. Kh. Kitaeva, JETP Lett. **118**, 395 (2023).
15. F. D'Angelo, Z. Mics, M. Bonn, and D. Turchinovich, Opt. Express **22**, 12475 (2014).
16. J. Qin, L. Xie, and Y. Ying, Food Chem. **224**, 262 (2017).
17. O. A. Smolyanskaya, N. V. Chernomyrdin, A. A. Konovko, et al., Prog. Quantum Electron. **62**, 1 (2018).
18. M. M. Nazarov, A. P. Shkurinov, E. A. Kuleshov, and V. V. Tuchin, Quantum Electron. **38**, 647 (2008).
19. I. E. Ilyakov, G. K. Kitaeva, B. V. Shishkin, and R. A. Akhmedzhanov, Opt. Lett. **42**, 1704 (2017).
20. I. E. Ilyakov, B. V. Shishkin, S. B. Bodrov, G. Kh. Kitaeva, M. I. Bakunov, and R. A. Akhmedzhanov, Laser Phys. Lett. **17**, 085403 (2020).
21. H. A. Hafez, X. Chai, A. Ibrahim, S. Mondal, D. Férachou, X. Ropagnol, and T. Ozaki, J. Opt. **18**, 093004 (2016).
22. J. Neu and C. A. Schmuttenmaer, J. Appl. Phys. **124**, 231101 (2018).
23. R. Burger, J. Frisch, M. Hübner, M. Goldammer, O. Peters, E. Rönneberg, and D. Wu, Sensors **21**, 3473 (2021).
24. P. U. Jepsen, J. Infrared Millim. Terahertz Waves **40**, 395 (2019).
25. O. S. Ahmed, M. A. Swillam, M. H. Bakr, and X. Li, J. Lightwave Technol. **28**, 1685 (2010).
26. R. Peretti, S. Mitryukovskiy, K. Froberger, M. A. Mebarki, S. Eliet, M. Vanwolleghem, and J.-F. Lampin, IEEE Trans. Terahertz Sci. Technol. **9**, 136 (2019).
27. T. Okada and K. Tanaka, Sci. Rep. **1**, 1 (2011).
28. W. Cai and V. Shalaev, *Optical Metamaterials* (Springer, New York, 2010).
29. V. G. Veselago, Sov. Phys. Usp. **10**, 509 (1967).
30. J. Pendry, A. Holden, D. Robbins, and W. Stewart, IEEE Trans. Microwave Theory Tech. **47**, 2075 (1999).
31. A. I. Musorin, A. V. Chetvertukhin, T. V. Dolgova, H. Uchida, M. Inoue, B. S. Luk'yanchuk, and A. A. Fedyanin, Appl. Phys. Lett. **115**, 151102 (2019).
32. V. Zubyuk, L. Carletti, M. Shcherbakov, and S. Kruk, APL Mater. **9**, 060701 (2021).
33. A. M. Chernyak, M. G. Barsukova, A. S. Shorokhov, A. I. Musorin, and A. A. Fedyanin, JETP Lett. **111**, 46 (2020).
34. R. Singh, W. Cao, I. Al-Naib, L. Cong, W. Withayachumnankul, and W. Zhang, Appl. Phys. Lett. **105**, 171101 (2014).
35. S. Han, M. V. Rybin, P. Pitchappa, Y. K. Srivastava, Y. S. Kivshar, and R. Singh, Adv. Opt. Mater. **8**, 1900959 (2020).
36. I. A. Novikov, M. A. Kir'yanov, A. Yu. Frolov, V. V. Popov, T. V. Dolgova, and A. A. Fedyanin, JETP Lett. **118**, 574 (2023).
37. M. A. Kiryanov, G. S. Ostanin, T. V. Dolgova, M. Inoue, and A. A. Fedyanin, JETP Lett. **117**, 196 (2023).
38. A. Yu. Frolov, M. R. Shcherbakov, and A. A. Fedyanin, Phys. Rev. B **101**, 045409 (2020).
39. B. I. Afinogenov, V. O. Bessonov, I. V. Soboleva, and A. A. Fedyanin, ACS Photon. **6**, 844 (2019).
40. N. Meinzer, W. L. Barnes, and I. R. Hooper, Nat. Photon. **8**, 889 (2014).
41. S. Shen, X. Liu, Y. Shen, J. Qu, E. Pickwell-MacPherson, X. Wei, and Y. Sun, Adv. Opt. Mater. **10**, 2101008 (2022).
42. X. Zang, B. Yao, L. Chen, J. Xie, X. Guo, A. V. Balakin, A. P. Shkurinov, and S. Zhuang, Light: Adv. Manuf. **2**, 148 (2021).
43. H.-T. Chen, W. J. Padilla, J. M. O. Zide, A. C. Gossard, A. J. Taylor, and R. D. Averitt, Nature (London, U.K.) **444**, 597 (2006).
44. I. Chatzakis, P. Tassin, L. Luo, N.-H. Shen, L. Zhang, J. Wang, T. Koschny, and C. M. Soukoulis, Appl. Phys. Lett. **103**, 043101 (2013).
45. Z. Xie, X. Wang, J. Ye, S. Feng, W. Sun, T. Akalin, and Y. Zhang, Sci. Rep. **3**, 3347 (2013).
46. S. Busch, B. Scherger, M. Scheller, and M. Koch, Opt. Lett. **37**, 1391 (2012).
47. L.-J. Cheng and L. Liu, Opt. Express **21**, 28657 (2013).
48. S. F. Busch, S. Schumann, C. Jansen, M. Scheller, M. Koch, and B. M. Fischer, Appl. Phys. Lett. **100**, 261109 (2012).
49. H. K. Tyagi and J. Gómez Rivas, J. Opt. **16**, 094011 (2014).

50. T. Wen, J. Tong, D. Zhang, Y. Zhu, Q. Wen, Y. Li, H. Zhang, Y. Jing, and Z. Zhong, J. Phys. D: Appl. Phys. **52**, 255303 (2019).
51. Q.-Y. Wen, Y.-L. He, Q.-H. Yang, P. Yu, Z. Feng, W. Tan, T.-L. Wen, Y.-X. Zhang, Z. Chen, and H.-W. Zhang, Adv. Mater. Technol. **5**, 1901058 (2020).
52. J. W. He, X. K. Wang, Z. W. Xie, Y. Z. Xue, S. Wang, and Y. Zhang, APL Photon. **2**, 076102 (2017).
53. J. Guo, T. Wang, H. Zhao, X. Wang, S. Feng, P. Han, W. Sun, J. Ye, G. Situ, H.-T. Chen, and Y. Zhang, Adv. Opt. Mater. **7**, 1801696 (2019).
54. G. Georgiou, H. K. Tyagi, P. Mulder, G. J. Bauhuis, J. J. Schermer, and J. G. Rivas, Sci. Rep. **4**, 3584 (2014).
55. Y. Shi, Q. li Zhou, C. Zhang, and B. Jin, Appl. Phys. Lett. **93**, 121115 (2008).
56. M. A. Kiryanov, A. Yu. Frolov, I. A. Novikov, P. A. Kipp, P. K. Nurgalieva, V. V. Popov, A. A. Ezhov, T. V. Dolgova, and A. A. Fedyanin, APL Photon. **7**, 026104 (2022).

Translated by the authors